*Textures and Microstructures*, Vol. 31, pp. 109–149
Reprints available directly from the publisher
Photocopying permitted by license only



# QUANTITATIVE PREDICTION OF COLD ROLLING TEXTURES IN LOW-CARBON STEEL BY MEANS OF THE LAMEL MODEL

P. VAN HOUTTE*, L. DELANNAY and I. SAMAJDAR†

*Department MTM, Katholieke Universiteit Leuven, de Croylaan 2, B-3001 Leuven, Belgium*

*(Received 20 July 1998)*

Rolling textures of low-carbon steel predicted by full constraints and relaxed constraints Taylor models, as well by a self-consistent model, are quantitatively compared to experimental results. It appears that none of these models really performs well, the best results being obtained by the Pancake model. A new model ("Lamel model") is then proposed as a further development of the Pancake model. It treats a stack of two lamella-shaped grains at a time. The new model is described in detail, after which the results obtained for rolling of low-carbon steel are discussed. The prediction of the overall texture now is quantitatively correct. However, the $\gamma$-fibre components are better predicted than the $\alpha$-fibre ones. Finally it is concluded that further work is necessary, as the same kind of success is not guaranteed for other cases, such as rolling of f.c.c. materials.

*Keywords:* Rolling texture; Steel; Polycrystal plasticity; Taylor model; Relaxed constraints model; Deformation banding

## 1. INTRODUCTION

It is well known that the crystallographic texture of a sheet material is modified by cold rolling. The final textures depend on the details of the rolling process as well as on the initial texture. Models which would be capable to predict these changes quantitatively would be of

* Corresponding author. Fax: +32 16 32 1990.
† Presently at the Department of Metallurgical Engineering & Materials Science, Indian Institute of Technology, Bombay, India.

considerable interest:

- Cold rolled sheets are often annealed to produce car body sheets. The annealing texture which is formed in this product is an important property. It depends on the texture and the microstructure of the cold rolled sheets. Details such as orientation-dependent dislocation densities or local strain heterogeneity play an important role. They cannot be measured easily, but a good model prediction might provide information on them, which would be helpful for the research effort spent on the understanding of annealing textures.
- The need is growing to incorporate deformation texture models in finite element (FE) software for the simulation of forming processes. Several FE software packages already take texture-based anisotropy into account. Some of them even try to simulate the texture evolution during the deformation. But a deformation texture prediction software which is quantitatively reliable does not really exist at present, so a research effort is necessary in this field.

The present paper describes contribution to this field. The work described is limited to low-carbon steel, and to rolling at room temperature as deformation process; but other materials and other processes will be studied in future work.

## 2. VALIDATION STRATEGY

The objective of the present work is to describe a new model which is supposed to make better quantitative predictions of the deformation texture. Hence a quantitative validation procedure is vital. Its principles will already be described at this stage of the paper. It consists in using the models to be tested for a particular rolling operation carried out on a sample of which the initial texture has been measured as well as the final texture and preferably also one or several intermediary textures. Orientation distribution functions (ODFs) are the only genuine quantitative representations of crystallographic textures, so the comparisons will be based on them. As an example, Fig. 1 shows the {110} and {100} pole figures and Fig. 2 the ODF of the initial texture (hot rolling texture). The ODF is made according to the Bunge (1982) convention on the basis of 4 incomplete pole figures measured by X-ray diffraction

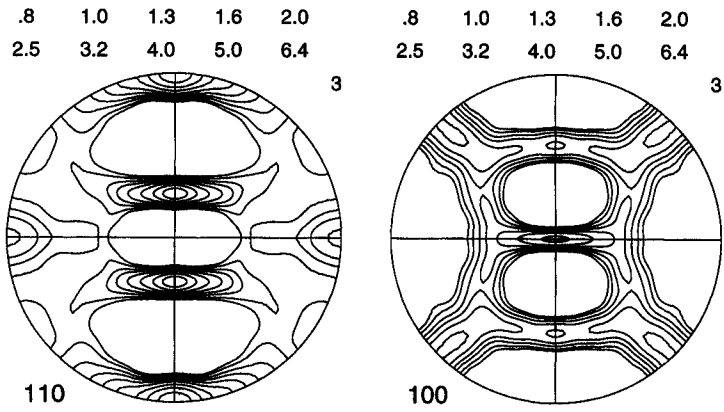


FIGURE 1 {1 1 0} and {1 0 0} pole figures of a hot rolled steel sheet.

({110}, {200}, {211} and {310}). A ghost correction procedure has been applied in order to obtain a strictly non-negative texture function (Van Houtte, 1991; 1992).

The starting material of this example has been rolled at room temperature. The thickness has been reduced by 70% (from 3 to 0.9 mm). This means that the true (longitudinal) strain was 1.2, and the corresponding von Mises equivalent strain 1.39. The final texture is shown by Figs. 3 and 4. At first sight, not much change has taken place when compared with the hot rolling texture (Figs. 1 and 2). From a qualitative point of view, both textures have the same features:[1] they are mainly characterised by an $\alpha$-fibre and a $\gamma$-fibre. The $\alpha$-fibre is a set of orientations described by $\{hkl\}\langle 110\rangle$; a longitudinal section of the fibre can be seen in a $\varphi_2 = 45°$ section (see Figs. 2, 4 and 5) at $\varphi_1 = 0°$ and $\Phi$ between 0° and 90°. The $\gamma$-fibre is described by $\{111\}\langle uvw\rangle$; a longitudinal section of it can also be seen in a $\varphi_2 = 45°$ section (see Figs. 2, 4 and 5) at $\Phi = 55°$ and $\varphi_1$ between 0° and 90°. This range consists of three equivalent segments, as shown by Fig. 5. Table I gives the meaning of the symbols used in the figure.

In order to see the difference between the textures, it is necessary to compare them quantitatively. This requires a plot such as Fig. 6, which

[1] Not all hot rolling textures of steel resemble cold rolling textures, see for example Vanderschueren *et al.* (1994).

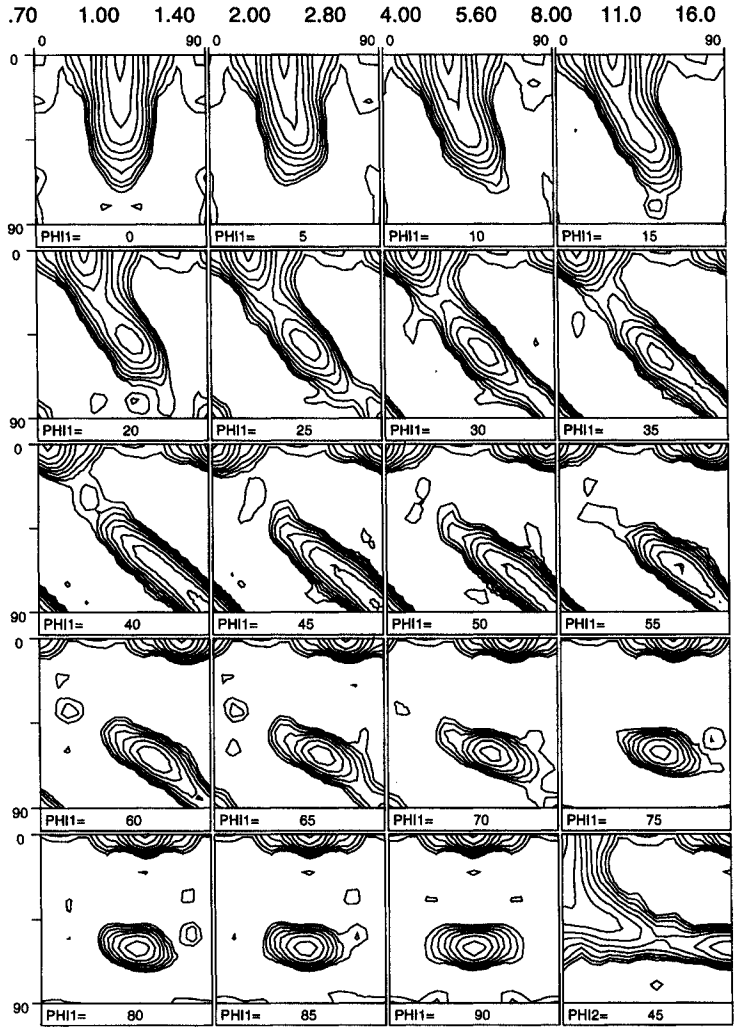


FIGURE 2 ODF of a hot rolled steel sheet.

shows the evolution of the maximum intensity along the skeleton line of the $\gamma$-fibre. Only one of the 3 equivalent ranges is shown. It should be noted that the maximal intensities along the fibre texture are not found at the exact position of the ideal $\gamma$-fibre. There are always deviations of a few degrees. For this reason, the intensity which Fig. 6 shows for a given value of $\varphi_1$ is not the intensity at the ideal position $\varphi_2 = 45°$ and $\Phi = 55°$,

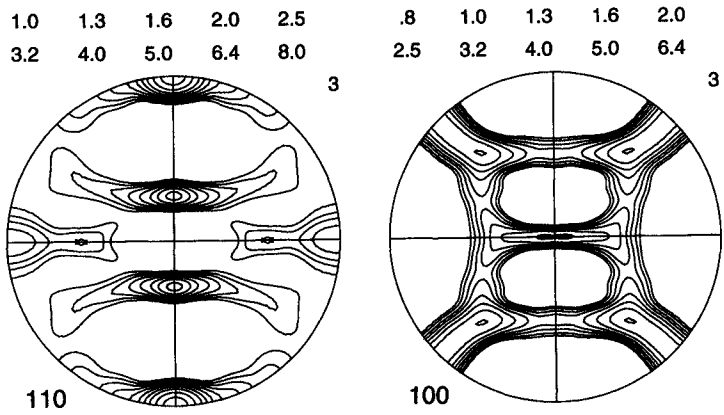


FIGURE 3 {1 1 0} and {1 0 0}pole figures of a cold rolled steel sheet.

but the maximal intensity found in a plane section of the fibre along a plane perpendicular to it ($\varphi_1 =$ constant plane).

The difference between the hot rolling and the cold rolling texture is made even clearer by Fig. 7, which for both textures shows the *r*-value (ratio between the transverse strain to the thickness strain in a tensile test) as a function of the angle to the rolling direction. The *r*-value has been calculated from the texture by means of the Taylor theory using $\{110\}\langle 111\rangle$ and $\{112\}\langle 111\rangle$ slip systems (see for example Schouwenaers *et al.*, 1994).

The same techniques will be used to compare the differences between the model predictions and the experimental results. But this requires a word about the textures which are involved in these simulations. We have computed the ODF of the initial texture (Figs. 1 and 2). It is a continuous function. However, most models operate on a texture represented by a set of discrete crystallite orientations (each with their own volume fraction), not on a continuous ODF. So a discretisation procedure has to be performed before a deformation texture prediction can be carried out. The "statistical" method described by Toth *et al.* (1991) has been chosen for this in the present work because it has been proven mathematically that this method leads to a "statistically unbiased" set of discrete orientations. In practice this means that the expected value (in the statistical sense) of a texture-dependent physical quantity such as a Taylor factor is equal whether it is calculated from

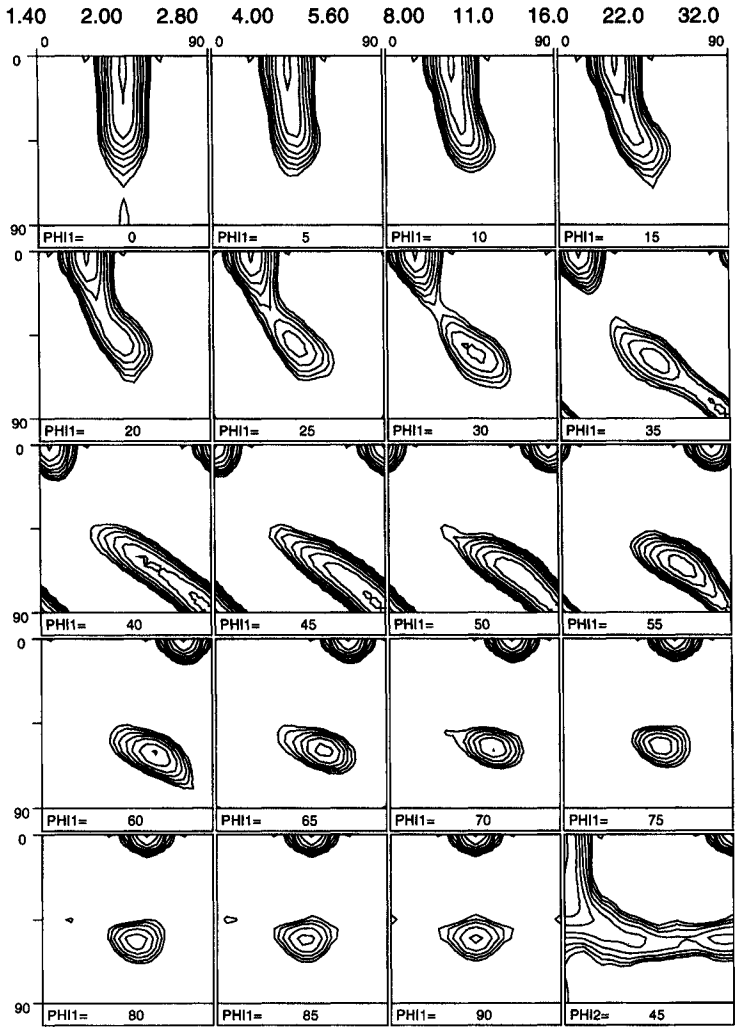


FIGURE 4 ODF of a cold rolled steel sheet.

the continuous ODF or from the discrete set of orientations derived from it. This property is an absolute necessity in a work like this, since the $r$-values obtained from the simulated textures must be compared to the $r$-values obtained from the experimental texture. This comparison would be meaningless if the discrete set of orientations was biased in a statistical sense.

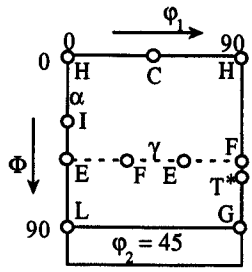


FIGURE 5 $\varphi_2 = 45°$ section of Euler space showing the $\alpha$- and $\gamma$-fibre of steel sheet textures. Table I shows the meaning of the symbols. It is seen that the orientations E and F have 2 equivalent representations in the $\varphi_2 = 45°$ section, with the result that the relevant range of the $\gamma$-fibre is represented 3 times in the section (EF, FE and EF).

TABLE I Ideal orientations shown in Fig. 5

| *Symbol* | *Conventional name* | *Miller indices* |
|---|---|---|
| C | Cube | (1 0 0)[0 0 1] |
| H | Rotated cube | (1 0 0)[0 $\bar{1}$ 1] |
| G | Goss | (1 1 0)[0 0 1] |
| T* | BCC Taylor | (11 11 8)[$\bar{4}$ $\bar{4}$ 11] |
| I | | (2 1 1)[0 $\bar{1}$ 1] |
| E | | (1 1 1)[0 $\bar{1}$ 1] |
| F | | (1 1 1)[0 1 2] |
| L | | (1 1 0)[1 $\bar{1}$ 0] |

At the end of a simulation, the result which still consists of a set of discrete orientations needs to be converted into a continuous texture function in order to be able to perform comparisons as shown by Fig. 6. The procedure is the following. Suppose the number of discrete orientations is $n$.

First, the $C$-coefficients of the following Gaussian distribution are generated for each of the $n$ crystallite orientations:

$$f_G(g) = \alpha \exp\left[-\left(\frac{\psi}{\psi_0}\right)^2\right] \tag{1}$$

in which $\psi$ is the angular distance between the crystallite orientation at the centre of the distribution (one of the $n$ orientations) and the orientation $g$ ($g =$ a set of Euler angles). The formulas for the $C$-coefficients

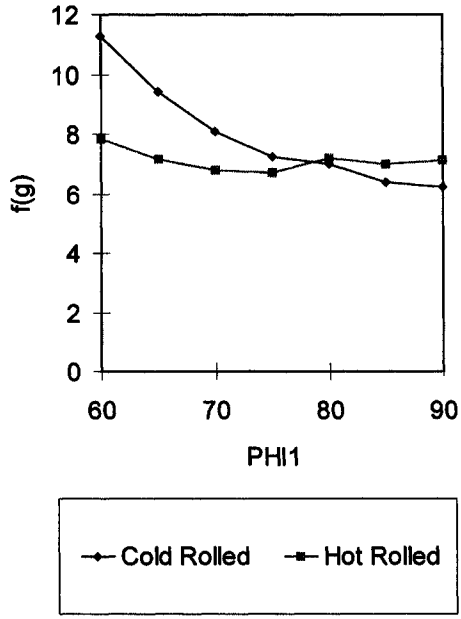


FIGURE 6 Evolution of the maximum intensity along the $\gamma$-fibre for the hot and cold rolling textures.

have been given by Bunge (1982). The value 7° is used for $\psi_0$. $\alpha$ is a factor which is adjusted in order to normalise $f_G(g)$.

Secondly, a continuous ODF is generated by making a linear combination of the $C$-coefficients of these $n$ Gauss distributions, using the same weighting factors as those assigned to the $n$ discrete orientations. The resulting ODF must then be normalised. The choice of 7° for $\psi_0$ is somewhat arbitrary, but for series expansion degrees of $l_{max} = 22$ or 32, it offers a reasonable compromise between angular resolution (the lower $\psi_0$, the better the resolution) and the suppression of undesired negative oscillations in the recalculated ODF. The meaning of $l_{max}$ is given by Bunge (1982). It is, however, a problem that the intensities of the ODF so obtained depend on the value of $\psi_0$, whereas the intensities of the ODF of the experimental textures (which must be compared to the simulated ODFs) are of course independent of it. In principle one could adjust the $\psi_0$ of the simulated textures to obtain a better quantitative agreement between simulated and measured textures (although such

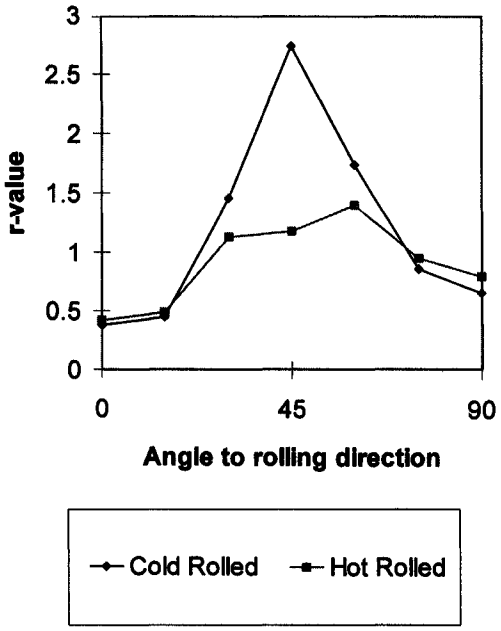


FIGURE 7 *r*-values in function of the angle to the rolling direction, as calculated from the hot rolling and the cold rolling steel texture.

adjusting was not done in the present work). So it would not be wise to attribute too much importance to the absolute value of the peak heights of the texture when comparing experimental and simulated ODFs; rather should one compare the profiles of the intensity distributions (as given, for example, by Fig. 6) which should show the same tendencies. For isolated peaks, one could also compare the weight of the peak (integral of the ODF in the range of the peak). However, for textures which are rather sharp, as is usually the case for deformation textures, the intensities of both the experimental ODF and the ones recalculated from the results of the simulation are limited by the power of resolution of the series expansion method. As a result and in spite of the foregoing discussion, their maximal intensities may be almost equal if the simulated and measured textures are almost equal.

A final principle used in the present work is that a deformation prediction made by a new model is never to be compared to an experimental result without also looking at the results of other models. Such a

procedure is the only one which ensures a serious assessment of the progress that a new model really represents. At the very least, one should include the results of the "Full Constraints Taylor–Bishop–Hill model", treated here as the "reference deformation texture prediction model", in the comparison.

## 3. PREVIOUS RESULTS

### 3.1. Short Description of some Older Models

A vast literature exist about modelling the plastic deformation of polycrystalline materials and predicting deformation textures. For a more complete list of references, we refer to a review paper (Aernoudt *et al.*, 1993); an interesting discussion of the validity of various models has been given by Leffers *et al.* (1988).

In most of these models, two elements can be discerned: a sub-model for the microscopic scale (*microscopic model*), and one for the transition from microscopic to macroscopic scale.

The *microscopic model* is basically the same for all the models which are of interest in the present work. It provides a relationship between, on the one hand, the strain rate and the rate of rigid body rotation (both combined in the velocity gradient tensor) of some microscopic volume element within a crystallite, and on the other hand, the slip rates, lattice rotation rates and deviatoric stress in that volume. The relationship is based on the laws of crystal plasticity in one form or another. Usually there is a kinematical relationship, which merely expresses the fact, that the microscopic velocity gradient $l_{ij}$ is the combined result of all slip processes which are simultaneously active. The following equation is obtained (Aernoudt *et al.*, 1993):

$$l_{ij} = \dot{\Omega}_{ij} + \sum_{s=1}^{N} b_i^s n_j^s \dot{\gamma}_s \tag{2}$$

in which $\dot{\Omega}_{ij}$ is the rate of rotation of the crystal lattice; $\dot{\gamma}_s$ is the slip rate on slip system $s$; $N$ is the total number of slip systems (f.c.c.: 12, i.e. $\{111\}\langle 110\rangle$; b.c.c.: 24, i.e. $\{110\}\{112\}\langle 110\rangle$); $b_i^s$ is the unit vector in slip direction and $n_j^s$ is the unit vector normal to the slip plane of slip

system $s$. $\dot{\Omega}_{ij}$ vanishes from Eq. (2) if the symmetric part is taken as

$$d_{ij} = \sum_{s=1}^{N} \tfrac{1}{2}(b_i^s n_j^s + b_j^s n_i^s)\dot{\gamma}_s \tag{3}$$

in which $d_{ij}$ is the symmetrical part of $l_{ij}$. Note that elastic strain rates are neglected, and that it is assumed that the volume does not change (i.e. $d_{11}+d_{22}+d_{33}=0$). As a result, Eq. (3) is a set of 5 independent equations (Aernoudt *et al.*, 1993). In general it is not known which slip systems are active before the equation is solved. This means that all $\dot{\gamma}_s$ must be considered to be unknowns. Since there are more unknowns than equations, the solution of the equation will not be unique. In general, there will be a large number of different sets of 5 non-zero $\dot{\gamma}_s$-values which all are solutions.[2] It is then clear that an additional assumption or procedure is needed in order to restrict the number of solutions. There are several variants of it. Taylor (1938) himself assumed that, of all possible solutions, the best is the one for which the internally dissipated frictional work is minimal:

$$\dot{W}^* = \sum_{s=1}^{N} \tau_s^c |\dot{\gamma}_s| = \text{Min} \tag{4}$$

in which $\tau_s^c$ is the critical resolved shear stress on slip system $s$. This variant of the microscopic model can be solved by means of linear programming (see for example Van Houtte, 1988). In the simplest case, the solution will be the set of 5 non-zero $\dot{\gamma}_s$-values which makes $\dot{W}^*$ minimal. However, there are also more complicated cases, for which we refer to the specialised literature (Aernoudt *et al.*, 1993; Leffers *et al.*, 1988; Van Houtte, 1988; Gil Sevillano *et al.*, 1980).

Once the slip rates have been found, the kinematical equation (2) is used in order to find $\Omega_{ij}$, the rate of rotation of the crystal lattice.

The 5 non-zero $\dot{\gamma}_s$-values also identify the active slip systems. The generalised Schmid law can then be written for them as

$$\sum_i \sum_j \tfrac{1}{2}(b_i^s n_j^s + b_j^s n_i^s)\sigma'_{ij} = \text{sign}(\dot{\gamma}_s)\tau_s^c. \tag{5}$$

[2] In addition to this, all positive linear combinations of the sets of 5 non-zero $\dot{\gamma}_s$ which are found, are also valid solutions.

Note that the left-hand side of this equation is the expression for the resolved shear stress $\tau_s^r$. Equation (5) represents a set of 5 linear equations from which the 5 independent components of the deviatoric stress $\sigma'_{ij}$ can be obtained.[3]

For the micro–macro transition, Taylor (1938) proposed to assume that the strain rate of all the crystallites of a polycrystalline material should be the same. This assumption is achieved by a more general assumption, which avoids the formation of holes and overlaps between the grains, and according to which the velocity gradients of all $l_{ij}$ microscopic volume elements should be the same and equal to the macroscopic velocity gradient, which in the case of rolling is given by:

$$[L_{ij}] = \begin{bmatrix} 1 & 0 & 0 \\ 0 & 0 & 0 \\ 0 & 0 & -1 \end{bmatrix} \dot{\varepsilon} \tag{6}$$

(at least for the centre plane of the rolling process). $\dot{\varepsilon}$ is a scalar parameter which represents the macroscopic strain rate, and of which the value can be arbitrarily chosen in the present context.

Such a model for which $l_{ij} = L_{ij}$ is called the Taylor–Bishop–Hill model or also, the "Full Constraints (FC) Model" in contrast to the "Relaxed Constraints Models" (see below). It has been widely discussed in literature (see for example (Taylor, 1938; Aernoudt *et al.*, 1993; Leffers *et al.*, 1988; Van Houtte, 1988; Gil Sevillano *et al.*, 1980)). For cubic metals, it is renowned to give good qualitative predictions of deformation textures in many (not all) cases. Some results will also be presented in the present paper.

Many authors (see for example Van Houtte, 1982; Kocks and Chandra, 1982; Honeff and Mecking, 1981) have proposed models which do not strictly enforce the condition $l_{ij} = L_{ij}$ but "relax" it for particular values of *ij*. Such models are called "*Relaxed Constraints (RC) models*". An example is the "Lath" model for rolling. It is supposed to be appropriate for elongated grains (Fig. 8). All

[3] In Eq. (5), the expression sign $(\dot{\gamma}_s)\tau_s^c$ can also be replaced by $\tau_s^c$ if the positive and the negative sense of each slip system are treated as separate slip systems. The slip rate on each active "slip system" must always be positive if this method is used. Each of the "generalised" slip systems may then have its own critical shear stress $\tau_s^c$ (positive values, to be used in Eqs. (4) and (5)), and they can be chosen differently for forward and backward slip on a given "physical" slip system.

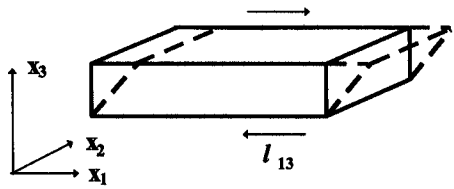


FIGURE 8 Schematic representation of a flat, elongated grain. In the case of rolling, $x_1$ would be the rolling direction, and $x_3$ the rolling plane normal. In the Lath version of the relaxed constraints model, the shear $l_{13}$ would be "relaxed".

components of the local velocity gradient tensor $l_{ij}$ must be equal to those of the macroscopic velocity gradient tensor given by Eq. (6), except the component $l_{13}$. The model must be made in such way that it yields the value of $l_{13}$ for which the work needed for the plastic deformation of the grain considered is minimal. This is achieved in the following way:

- the value of $l_{13}$ considered as unknown. Because of this, the value of

$$d_{13} = \frac{l_{13} + l_{31}}{2} \tag{7}$$

  is also unknown in advance (although $l_{31}$ is still prescribed);
- as a result, the equation for $d_{13}$ in the set given by Eq. (3) has to be dropped. The remaining 4 equations can then be solved in combination with Eq. (4). The solution now takes the aspect of 4 non-zero slip rates instead of 5. Once these slip rates are found, the equation for $d_{13}$ in the set of Eq. (3) can be used to calculate $d_{13}$, after which $l_{13}$ can be solved from Eq. (7).

It has been shown by Van Houtte (1982) that the solutions for the slip rates found by this theory are the same as those found by a "mixed boundary conditions" type of Bishop–Hill theory which would assume that $\sigma'_{13}$ is zero and that $d_{13}$ is not imposed (Kocks and Chandra, 1982). Various justifications have been proposed for these theories, all of which in one way or the other express the idea that in the case of flat, elongated grains, the interactions between neighbouring grains are incapable of building the necessary stress level which would be needed for a full enforcement of the macroscopic strain upon the considered grain (Van Houtte, 1982; Kocks and Chandra, 1982; Honeff and Mecking, 1981).

The Pancake model for rolling is another version of the RC theory, which is more frequently used than the Lath version. Not only the shear $l_{13}$ (Fig. 8), but also the shear $l_{23}$ is relaxed. According to this theory, 3 slip systems will be activated in each grain. The corresponding "mixed boundary conditions" Bishop–Hill theory is the one for which both $\sigma'_{13}$ and $\sigma'_{23}$ are zero.

Whatever justification is used for an RC theory, the choice of the $l_{ij}$-components to be relaxed remains arbitrary and would, for each particular application, depend on a subjective judgement of the nature of the microscopic stress/strain distribution. It is therefore logical, to try to find a theory which would make this choice automatically. Such theory might be called "generalised RC model", such as the theory proposed by Van Houtte and Rabet (1997). However, their theory belongs in fact to the class of "*self consistent models*" which treat each grain in turn as if it were an ellipsoidal inclusion embedded in a matrix of which the plastic properties (tangent moduli) are the same as those of the entire polycrystal. The main difference between the "generalised RC model" and the older visco-plastic self-consistent model proposed by Molinari *et al.* (1987) is that the former uses a different method to estimate the reaction stresses built up by the matrix against grain relaxations. The former model probably overestimates these reactions stresses, whereas the latter underestimates them, especially for materials with a small strain rate sensitivity exponent (Van Houtte, 1995).[4] For more details about self-consistent models in general, we refer to the specialised literature (e.g. Van Houtte and Rabet, 1997; Molinari *et al.*, 1987).

### 3.2. Results of the Older Models

The cold rolling textures shown by Figs. 3 and 4 have been simulated using the FC Taylor–Bishop–Hill model, two variants of the RC model (Lath and Pancake) and the Generalised Relaxed Constraints model as an example of a self-consistent model. The procedures described in Section 2 "Validation Strategy" have been used. The hot rolling texture

[4]This comment refers to the reaction stresses that a hypothetical matrix with average plastic properties would have against a grain. These reaction stresses are different from those in which a particular grain in a polycrystal would experience from its neighbours, because the latter do not have the average plastic properties of the polycrystal.

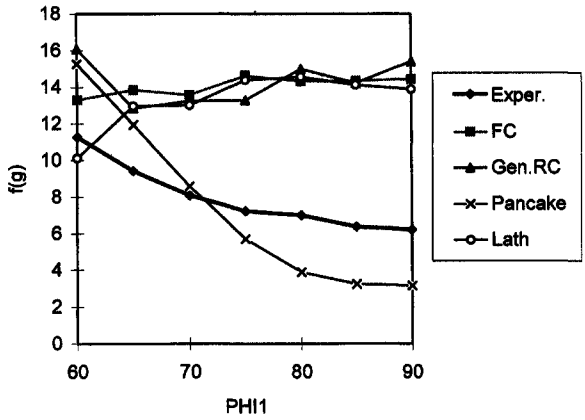


FIGURE 9 Evolution of the maximum intensity along the $\gamma$-fibre for the experimental cold rolling texture and for the results of the Full Constraints model (FC), the Lath and Pancake versions of the Relaxed Constraints models, and the Generalised Relaxed Constraints model.

shown by Figs. 1 and 2 has been discretised into 400 crystallite orientations and then used as initial texture. The resulting ODFs and pole figures have been published elsewhere (Van Houtte, 1997). Qualitatively, all these simulated textures present the main features of BCC rolling textures as described in Section 2, although some pole figures look rather distorted because of angular shifts of the positions of the skeleton lines of the $\gamma$-fibre. A quantitative comparison can be made by means of the intensity distribution along the fibre (Fig. 9). This figure is similar to Fig. 6 described in Section 2. Figure 10 compares the $r$-values as calculated from the texture by means of the FC Taylor theory.

Inspection of Fig. 9 reveals that

(i) the result of the FC Taylor–Bishop–Hill theory (still regarded as the "reference model") does not capture the main tendency of the evolution of the maximum intensity along the $\gamma$-fibre of the experimental cold rolling texture, namely a decrease from 11.3 at E ($\phi_1 = 60°$) to 7 at F ($\phi_1 = 90°$). Instead, the maximum intensity begins at 13.3 at E and slightly *increases* until a value of 14.3 at F;

(ii) the Lath model (RC) predicts an even more increasing tendency than the FC model;

(iii) the result of the Generalised RC model does not differ much from the result of the FC model. Only at E, the intensity is significantly

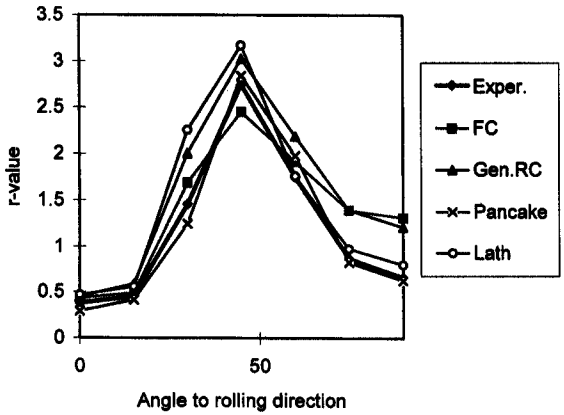


FIGURE 10 *r*-values in function of the angle to the rolling direction, as calculated from the experimental cold rolling steel texture and from the textures simulated by the various models (see the subtitle of Fig. 9).

higher (16 instead of 13.3). A decreasing tendency is observed between $\phi_1 = 60°$ and 65° only; from $\phi_1 = 60°$ until 90°, the tendency is slightly increasing, as for the FC model;

(iv) only the result of the Pancake model (RC) shows a decreasing tendency, which however is exaggerated as compared to the experimental result.

Inspection of Fig. 10 confirms that the best results are obtained by the Pancake version of the RC model, although this model is much less complex than the Generalised Relaxed Constraints model. This result will be used as the basis of the reasoning underlying the development of a new model in the next section.

## 4. THE LAMEL MODEL

### 4.1. Introduction

In Section 3.2, it was found that the comparatively simple Pancake model makes better predictions of the rolling texture of a low-carbon steel than the Generalised Relaxed Constraints model, although the theoretical basis of the latter model seems much sounder (see Section 3.1). From a theoretical point of view, inspection of Fig. 9 suggests that

- the FC model cannot reproduce the experimentally observed decrease of intensity observed between E and F along the $\gamma$-fibre;
- completely relaxing the component $l_{13}$ as is done in the Lath model (see Section 3.1 and Fig. 8) does not help;
- a limited relaxation of both $l_{13}$ and $l_{23}$ as is done in the Generalised Relaxed Constraints Method (a self-consistent method) does not help much either, although such limited relaxation seems scientifically much more sound than a completely free relaxation;
- a completely free relaxation of both $l_{13}$ and $l_{23}$ as is done by the Pancake model, does reproduce the decrease of intensity, but overestimates it.

All this suggests that one could get good agreement between the experimental texture and the model predictions by "fine-tuning" the Generalised Relaxed Constraints model. Obviously, it does not give enough freedom to $l_{13}$ and $l_{23}$, so perhaps better results would be obtained if the reaction stresses built up by the matrix against grain relaxations was artificially reduced. Maybe so, but this is not satisfying from a scientific point of view. Indeed, in the present version of the Generalised Relaxed Constraints model, the reactions stresses are calculated on the basis of sound micromechanical assumptions. This physical basis would be lost if the reaction stresses were artificially reduced. In future work the present authors may perhaps use this method anyway. But in the present work, it is preferred to improve agreement between simulated and experimental results by proposing a different model, which may look primitive as compared to a "fine-tuned" Generalised Relaxed Constraints model, but which is based on precisely defined physical assumptions.

In the stage of designing the new model, the *objective* set for was to give more freedom to $l_{13}$ and $l_{23}$ than the Generalised Relaxed Constraints model does, but not the unlimited freedom given by the Pancake model. As explained above, a better agreement between the observed and simulated intensity distribution of the texture can then be expected. The main question was: is it possible to imagine a heterogeneous deformation pattern at grain level, which is physically acceptable and which at the same time would achieve the objective described above. The present authors believe that the *lamel* model which will be described below is such model.

### 4.2. Description of the Model

The microstructure of a polycrystalline material is modelled as if it were a lamellar structure consisting of nicely stacked elongated grains (Fig. 11). Initially, the crystallite orientation of each of the grains shown in Fig. 11 is an orientation taken at random using the ODF $f(g)$ of the material as probability distribution function. Now, instead of treating the grains one by one, as would be done by the FC Taylor theory, stacks of two grains each are considered, such as "grain 1" and "grain 2" shown by Fig. 11.

The Taylor assumption of homogenous strain is now applied to each of these stacks as a whole, and not to the individual grains of which it consists. It means that the velocities (displacements per unit time) of the points A, B, E, F shown in Fig. 11 must be the same as they would have according to a FC Taylor model. However, this is not required for the points C and D: the components $v_1$ and $v_2$ of their velocities (i.e., the components parallel to the interface plane between grain 1 and grain 2) are left free, whereas the components $v_3$ (normal to the interface plane) must keep the same value as in the FC Taylor theory.

Figure 12 then illustrates how the shape of the grains then would have evolved after an increment of time $\Delta t$: due to an horizontal shift $\Delta_1$ of the points C and D relative to the points A/E and B/F, respectively, opposite shears $-\Delta\gamma_{13}^{L}$ and $\Delta\gamma_{13}^{L}$ will develop in grain 1 and grain 2, respectively:

$$\Delta\gamma_{13}^{L} = \Delta_1/h \tag{8}$$

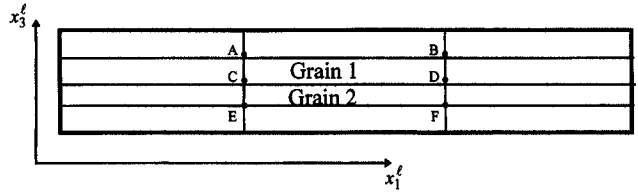


FIGURE 11 Geometrical model used by the Lamel model for the microstructure for a single-phase polycrystalline material. In case of rolling, the figure represents a longitudinal section. For the examples treated in the present paper, the axes $x_1^\ell$ and $x_3^\ell$ of the lamellae reference system coincide with the rolling direction and the rolling plane normal, respectively.

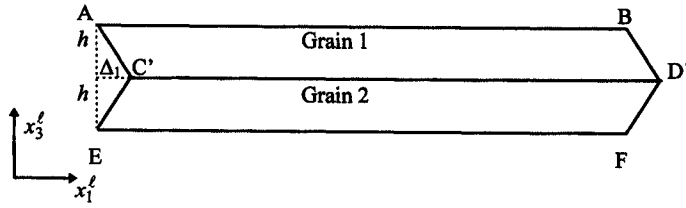


FIGURE 12 Shape of the grains 1 and 2 after a time $\Delta t$, if $\dot{\gamma}_{13}^{L}$ is non-zero.

(see Fig. 12). The superscript L refers to the "Lamel" model. This shear is an additional shear as compared to the shear which would be imposed by the FC Taylor theory (i.e., the component 13 of the macroscopic shear, which is zero in case of a perfect plane strain deformation, but might be different from zero when redundant shear rates exist, such as close to the surface in rolling). In a similar way, shears $-\Delta\gamma_{23}^{L}$ and $\Delta\gamma_{23}^{L}$ can also develop in grains 1 and 2, respectively.

The Lamel model in its present form will compute the shear rates $\dot{\gamma}_{13}^{L}$ and $\dot{\gamma}_{23}^{L}$ and take them into account for the calculation of the plastic work and the lattice rotation in the two grains (see below). However, it will not use them to compute $\Delta\gamma_{13}^{L}$ and $\Delta\gamma_{23}^{L}$ from the length of a time increment $\Delta t$ and use them to modify the geometrical model by changing the shapes of grains 1 and 2 by new shapes as shown in Fig. 12 after each simulated time increment. This was judged too complicated. Instead, Fig. 11 is supposed to remain an adequate geometrical model for the microstructure for all successive deformation increments to be simulated.

The shear rates $\dot{\gamma}_{13}^{L}$ and $\dot{\gamma}_{23}^{L}$ will be calculated on the basis of the principle of minimum plastic work applied to a set of two grains taken together. For the rest, the Taylor equation (3) is applied to each of the two crystallites. This makes a total of 10 geometrical constraints, however with 2 additional degrees of freedom ($\dot{\gamma}_{13}^{L}$ and $\dot{\gamma}_{23}^{L}$). As a result, the minimum number of active slip systems is 8 for the two crystallites together, or 4 on average per crystallite.

It is clear that the shifts $\Delta_1$ and $\Delta_2$, which are implied by this model, will cause misfits between each stack of two grains and its environment. These misfits will create stress and strain localisations which in a real material would tend to reduce the shear rates and $\dot{\gamma}_{13}^{L}$ and $\dot{\gamma}_{23}^{L}$. This effect is not explicitly taken into account by the model. As a result, one may expect that the lamel model would overestimate $\dot{\gamma}_{13}^{L}$ and $\dot{\gamma}_{23}^{L}$.

In general, the counteracting effect of the misfit strains has the same nature as in a Pancake RC model, or in the Generalised Relaxed Constraints model. There are, of course, differences:

- the effects due to misfit strains are much larger in case of the Pancake RC model. Suppose indeed that we would apply such model to grain 1 and grain 2 of Fig. 11. Let us assume that the velocities of points A and B, and E and F would be those that would be expected in a FC Taylor model. The velocities of C and D would then be different for grain 1 and for grain 2 (as each grain can have its own "relaxed" shear rates $\dot{\gamma}_{13}^{RC}$ and $\dot{\gamma}_{23}^{RC}$). As a result, the misfit strains would include an "infinite shear" at the interface between the two grains, in other words, grain boundary sliding. Since this takes place along a large surface as compared to the surfaces AE and BF, the plastic work associated to it would be probably considerably higher than the plastic work associated with the misfits shown at AC'E and BD'F in Fig. 12. The resulting effect counteracting $\dot{\gamma}_{13}^{RC}$ and $\dot{\gamma}_{23}^{RC}$ would consequently also be much higher than in the case of the lamel model. Since the Pancake RC model does not take the counteracting effect into account, it is expected to overestimate the absolute values of $\dot{\gamma}_{13}^{RC}$ and $\dot{\gamma}_{23}^{RC}$ much more than the Lamel model would overestimate $\dot{\gamma}_{13}^{L}$ and $\dot{\gamma}_{23}^{L}$.
- The Generalised Relaxed Constraints model also liberates $\dot{\gamma}_{13}^{RC}$ and $\dot{\gamma}_{23}^{RC}$. But in contrast to the Pancake model, it does take the counteracting effect of the misfit strains into account. As explained above, this effect is rather strong, and so the Generalised Relaxed Constraints model reduces $\dot{\gamma}_{13}^{RC}$ and $\dot{\gamma}_{23}^{RC}$ too much. One may wonder why the Lamel model would not do so as well. Indeed, it can very well be that in the Lamel model, $\dot{\gamma}_{13}^{L}$ and $\dot{\gamma}_{23}^{L}$ are very small or even zero, because values for them which would reduce the plastic work in grain 1 might very well *increase* the plastic work in grain 2 or vice versa. However, the Lamel model would on the opposite recognise certain energetically favourable configurations, for example when grains 1 and 2 would happen to have such crystallite orientations that the same values of $\dot{\gamma}_{13}^{L}$ and $\dot{\gamma}_{23}^{L}$ would reduce the plastic work in both grain 1 and grain 2. In contrast to this, the Generalised Relaxed Constraints would not be able to recognise these favourable configurations, since it looks only at one grain at a time.

### 4.3. Mathematical Treatment of a Stack of Two Grains

The Einstein summation convention will be used in this section, unless otherwise stated. The kinematical equations (2) and (3) still hold for grain 1 as well as for grain 2, but not the condition $l_{ij} = L_{ij}$. The latter is replaced by:

$$l_{ij}^G = L_{ij} - R_{rij}^G \dot{\gamma}_r^L \tag{9}$$

The superscript $G$ is a variable which can take the values 1 and 2, and which indicates Grain 1 or Grain 2. The superscript L is not a variable and refers to the Lamel model. $r$ takes the values 1 and 2:

$$[R_{1ij}^1] = \begin{bmatrix} 0 & 0 & 1 \\ 0 & 0 & 0 \\ 0 & 0 & 0 \end{bmatrix} \quad \text{and} \quad R_{1ij}^2 = -R_{1ij}^1, \tag{10}$$

$$[R_{2ij}^1] = \begin{bmatrix} 0 & 0 & 0 \\ 0 & 0 & 1 \\ 0 & 0 & 0 \end{bmatrix} \quad \text{and} \quad R_{2ij}^2 = -R_{2ij}^1. \tag{11}$$

The $\dot{\gamma}_{13}^L$ and $\dot{\gamma}_{23}^L$ which were used in Section 4.2 are equal to $\dot{\gamma}_1^L$ and $\dot{\gamma}_2^L$, respectively. Note that it is assumed here that a reference system is used of which the axes $x_1^\ell$ and $x_2^\ell$ are parallel to the lamella planes (see Figs. 11 and 12). We will call this reference system the *lamella reference system.* For the application to rolling of a b.c.c. material with elongated grains, which will be discussed in the present work, it is also the sample reference system. However, future applications may be worked out for which the lamella reference system and the sample reference system may be different from each other.

The symmetrical part of Eq. (9) is:

$$d_{ij}^G = D_{ij} - N_{rij}^G \dot{\gamma}_r^L \tag{12}$$

in which the $N_{rij}^G$ are the symmetrical parts of the $R_{rij}^G$:

$$N_{rij}^G = \frac{1}{2}(R_{rij}^G + R_{rji}^G). \tag{13}$$

Eq. (3) may be used again if a superscript $G$ is added, because each grain has its own slip rates $\dot{\gamma}_s^G$. Besides, the multipliers of $\dot{\gamma}_s$ in Eq. (3) also depend on $G$, since the two grains have a different lattice orientation. Let us calculate these multipliers in the *crystal reference system* (for the meaning of $s$, $b$ and $n$, see the comment after Eq. (2)):

$$M_{sij}^{C} = \tfrac{1}{2}(b_i^{Cs} n_j^{Cs} + b_j^{Cs} n_i^{Cs}) \quad \text{(no summation over } s\text{)}. \tag{14}$$

The superscript C is not a variable; it refers to the crystal reference system. There is no need to use a superscript $G$ (to distinguish between grain 1 and grain 2) because as long as the two grains belong to the same phase, the values of $M_{sij}^{C}$ are the same for both grains. However, after transforming these $M$-coefficients to the lamella reference system, they will have different values for grain 1 and for grain 2, and we will have to use the superscript $G$ again. Equation (3) will now become (using also Eqs. (12) and (13)):

$$M_{sij}^{G} \dot{\gamma}_s^G + N_{rij}^{G} \dot{\gamma}_r^{L} = D_{ij} \quad \text{(no summation over } G\text{)}, \tag{15}$$

$s$ runs from 1 to $N$ (the number of slip systems). There is an equation for each grain (G 1 or 2) and for each value of $ij$. In total this makes 12 equations, of which only 10 are independent because of the assumption of incompressibility.[5] There are $2N+2$ unknown $\dot{\gamma}_s^G$ and $\dot{\gamma}_r^{L}$. Since $N=12$ for f.c.c. metals and 24 for b.c.c. metals, there will usually be multiple solutions. An additional criterion such as Eq. (4) will be used to restrict the choice of solutions. This additional criterion will state that the virtual frictional work dissipated in grains 1 and 2 *taken together* must be minimal:

$$\dot{W}_{1,2}^{*} = \tau_s^{cG} |\dot{\gamma}_s^G| + \tau_r^{L} |\dot{\gamma}_r^{L}| = \text{Min} \tag{16}$$

$\tau_s^{cG}$ is the critical resolved shear stress on slip system $s$ in grain $G$. $\tau_r^{L}$ is a possible frictional resistance against the relaxation $\dot{\gamma}_r^{L}$; in the basic version of the Lamel model, it is zero. Note that in the present analysis, it was assumed that the volumes of grain 1 and grain 2 are equal. A generalisation for grains with different volumes can easily be made.

[5] The equation for $ij = 33$ could for example be dropped for each of the two grains.

The minimisation problem consisting of finding the values of $\dot{\gamma}_s^G$ and $\dot{\gamma}_r^L$ which minimise $\dot{W}_{1,2}^*$ (Eq. (16)) while satisfying the 10 independent equations (15) can be solved by means of linear programming techniques, in a similar way as the FC Taylor theory (Van Houtte, 1988). In that case, it is convenient to write the 10 independent equations of Eq. (15) in matrix form. The coefficient matrix of these equations then has the following general structure:

$$[A] = \begin{bmatrix} [M_{sij}^1] & [0] & [N_{rij}^1] \\ [0] & [M_{sij}^2] & [N_{rij}^2] \end{bmatrix}. \tag{17}$$

In a sub-matrix such as $[M_{sij}^1]$, $s$ stands for the column-index and $ij$ (after contraction to a single index) for the row index. The column matrix with the unknowns consists of the set $\dot{\gamma}_s^1$ first, then the set $\dot{\gamma}_s^2$ and finally the two relaxations $\dot{\gamma}_r^L$.

Even while minimising $\dot{W}_{1,2}^*$(Eq. (16)), multiple solutions are found for $\dot{\gamma}_s^G$. The code which currently has been developed only looks for one solution. The values of $\dot{\gamma}_r^L$ which are part of this solution are then introduced in Eq. (9) in order to find $l_{ij}^G$ for grain 1 as well as for grain 2. In other words, the Lamel-routine which solves Eqs. (15) while minimizing $\dot{W}_{1,2}^*$(Eq. (16)) is only used to calculate the grain relaxations. As a result, the shape change of each of the two grains is then known. This shape change is then passed on to an existing routine for solving the FC Taylor theory, which treats grain 1 and grain 2 separately and has the task of finding the slip rates and lattice rotations. It does not use the values of the slip rates already found by the Lamel-routine, but calculates them again; this time making a particular choice among all possible solutions. This FC Taylor routine is based on an exponential expression for the single crystal yield locus (Eq. (18)) given by Van Houtte and Rabet (1997).

In a similar way as for the FC Taylor theory (Van Houtte, 1988), the "simplex multipliers" obtained after applying the linear programming technique to Eqs. (15) and (16) can be identified with the deviatoric stresses in the two grains. This can be illustrated in the following way. A typical solution of the linear programming problem would assign a non-zero value to 10 of the $2N+2$ unknowns $\dot{\gamma}_s^G$ and $\dot{\gamma}_r^L$. The other ones are set to zero. Let $\dot{\gamma}_4^1$ for example be such a non-zero solution. According to linear programming techniques, a set of 10 simplex

multipliers $\pi_p$ (the index $p$ corresponds to the rows of matrix $A$, Eq. (17)) exists which are such that the sum of the products $\pi_p A_{p4}$ is equal to the corresponding factor in the functional to be optimised (Eq. (16)). This factor is $\text{sign}(\dot{\gamma}_4^1)\tau_4^{c1}$. It is seen in Eq. (17) that the coefficients $A_{p4}$ are zero for rows corresponding to grain 2. As a result, the sum of the products $\pi_p A_{p4}$ only contains terms related to grain 1, and can be written as follows (using non-contracted indices):

$$\pi_{ij}^1 M_{4ij}^1 = \text{sign}(\dot{\gamma}_4^1)\tau_4^{c1}. \tag{18}$$

Similar expressions exist for all active slip systems, as well for grain 1 as for grain 2. If the $\pi_{ij}^G$ are identified with the deviatoric stresses $\sigma_{ij}'^G$ in the grain $G$, then the expressions (18) merely state, that for an active slip system, the resolved shear stress must be equal to the critical resolved shear stress in the grain.

However, 2 of the 10 non-zero values in the solutions may belong to the set of relaxations $\dot{\gamma}_r^L$. They then come in the place of ordinary slip rates $\dot{\gamma}_s^G$, either of grain 1 or of grain 2. As a result, a grain may have 5, 4 or 3 active slip systems, depending on the solution. Let us assume that a solution is found in which $\dot{\gamma}_1^L$ is non-zero. The simplex multiplier property leads to the following condition (identifying the simplex multipliers with the deviatoric stresses):

$$\sigma_{ij}'^1 N_{1ij}^1 + \sigma_{ij}'^2 N_{1ij}^2 = \text{sign}(\dot{\gamma}_1^L)\tau_r^L. \tag{19}$$

The values of $N_{1ij}^1$ and $N_{1ij}^2$ have been given above (Eqs. (10), (11) and (13)). Elaborating Eq. (19) then leads to:

$$\sigma_{13}'^1 - \sigma_{13}'^2 = \text{sign}(\dot{\gamma}_1^L)\tau_r^L. \tag{20}$$

As already mentioned above, $\tau_r^L$ is zero for the basic version of the Lamel model. Equation (20) then simply means, that if $\dot{\gamma}_{13}^L$ alias $\dot{\gamma}_1^L$ is relaxed, $\sigma_{13}'$ must be the same in both grains. It means that as far as this shear stress is concerned, relaxation implies the establishment of stress equilibrium at the boundary between grain 1 and grain 2.

In a similar way, $\sigma_{23}'$ must be the same in both grains when $\dot{\gamma}_{23}^L$ alias $\dot{\gamma}_2^L$ is relaxed.

## 4.4. Simulation of a Deformation Texture

### *4.4.1. Discretisation of the Initial Texture*

For each stack, the orientations of grain 1 and grain 2 should be taken (separately) at random in such way that the probability that a certain crystallite orientation $g$ chosen is equal to $f(g)$, the ODF of the initial texture. Care should be taken that the "sample symmetry" as defined by Bunge (1982) is not implemented in this ODF The reason is that crystallite orientations such as $(3\,2\,1)[\bar{4}\,3\,6]$, $(3\,2\,1)[4\,\bar{3}\,\bar{6}]$, $(\bar{3}\,\bar{2}\,\bar{1})[4\,\bar{3}\,\bar{6}]$ and $(\bar{3}\,\bar{2}\,\bar{1})[\bar{4}\,3\,6]$ (an example for cubic material) must each have a chance to be generated from the ODF. In case of orthorhombic sample symmetry (rolled or rolled and annealed material), these crystallite orientations are equivalent with respect to the sample symmetry, because they can be derived from each other by 180° rotations around the sample symmetry axes $x_1$, $x_2$ or $x_3$. But they are physically different orientations, and each of them should have a chance to be generated during the discretisation process. If one uses ODF and discretisation software in which the orthorhombic sample symmetry is implemented, then most probably of the series given above, only $(\bar{3}\,\bar{2}\,\bar{1})[4\,\bar{3}\,\bar{6}]$ will have a chance to be generated,[6] not the other ones.

Why this is important can be illustrated by means of the following example. Suppose that $(\bar{3}\,\bar{2}\,\bar{1})[4\,\bar{3}\,\bar{6}]$ happens to be chosen as the lattice orientation of grain 1 and $(\bar{3}\,\bar{2}\,\bar{1})[\bar{4}\,3\,6]$ for grain 2. So by accident, the crystallite lattice of grain 2 is the mirror image of that of grain 1 with respect to the rolling plane. Figure 12 shows that if a relaxation shear of the type $\Delta\gamma^{L}_{13}$ takes place in grain 2, then an opposite relaxation $-\Delta\gamma^{L}_{13}$ takes place in grain 1. If the shear $\Delta\gamma^{L}_{13}$ causes a diminution of the plastic work in grain 2, then the opposite shear $-\Delta\gamma^{L}_{13}$ will cause the same diminution of the plastic work in grain 1. The reason for this is that the lattices of both grains are each other's mirror image with respect to C′D′ (Fig. 12). Due to this synergetic effect, the model will be driven to strongly promote this kind of relaxation. However, if the discretisation software has replaced the orientation of grain 2 by $(\bar{3}\,\bar{2}\,\bar{1})[4\,\bar{3}\,\bar{6}]$ because of "symmetric equivalence", then both grains will have the *same* orientation. Any reduction of plastic work caused by a possible $\Delta\gamma^{L}_{13}$ in

[6] Because it is the only one of the four which has Euler angles which fall all three in the range from 0° to 90°, the conventional range for ODF with orthorhombic sample symmetry.

grain 2 will be compensated by an increase of plastic work caused by $-\Delta\gamma_{13}^{L}$ in grain 1, and it is very likely that the Lamel model would not generate any relaxation at all, although in fact, a strong relaxation should be produced. In fact, the model would hardly ever recognise configurations of grain 1 and grain 2 which strongly promote relaxation.

The following procedure has been followed by the present authors:

(i) in case the $C$-coefficients of the initial texture have a built-in orthorhombic sample symmetry, they are converted to a set without this symmetry using the program ROTTEX from the MTM-FHM package (Van Houtte, 1992);
(ii) the program CALCODF from MTM-FHM package was then used to generate the ODF on a grid in Euler space with a 0–360° range for $\varphi_1$, and 0–90° ranges for $\varphi_2$ and $\Phi$ (cubic material).
(iii) the "statistical discretisation method" described by Toth and Van Houtte (1992) was then used to generate a set of 2000 or 5000 crystallite orientations in totally random order. It was seen to it that all crystallite orientations generated had the same volume fraction, which can easily be achieved by the "statistical method".
(iv) these were then subdivided in 1000 or 2500 pairs representing the orientations of grain 1 and grain 2 in the stacks to be processed by the Lamel model.

### *4.4.2. Evolution of the Lamel Orientation*

The longitudinal direction of the lamella (Fig. 11) is the axis $x_1^{\ell}$ of the "lamella reference system" (see Section 4.3), whereas $x_3^{\ell}$ is normal to the plane of the lamellae. Most equations given in Section 4.3 were expressed in this lamella reference system. For the example of cold rolling of a b.c.c. metal, which is worked out in the present paper, it is assumed that the grains are elongated in the rolling direction, and the "lamella system" is identical with the sample system. However, there may be applications for which a distinction must be made between the lamella system and the sample reference system. In such cases, a description of the orientation of the lamella system with respect to the sample reference system would be needed, as well as a mathematical model for the evolution of this orientation. Many approaches can be imagined for this. In the current version of the software for the "Lamel model", the

following model is implemented:

(i) the grains, or other microstructural features which one wants to treat as "lamella", are described by ellipsoids. For an equiaxed material, these may be spheres. It is assumed that in the polycrystal, all such ellipsoids have the same shape and the same orientation. The axis $x_1^\ell$ of the "lamella reference system" is then is defined as the *longest* symmetry axis of the ellipsoid, whereas the axis $x_3^\ell$ is the shortest.

(ii) the orientations of the axes $x_i^\ell$ with respect to the sample system is described by Euler angles; the half-lengths of these axes are called $c_i$.

(iii) at need, this description by Euler angles is converted in a representation by means of a tensor **C**, which stands for the coefficients of an analytical equation describing the ellipsoid:

$$x_i C_{ij} x_j = 1. \tag{21}$$

This equation is expressed in the sample reference system. $C_{ij}$ is a symmetrical matrix. Its eigenvectors are parallel to the axes $x_i^\ell$, and its eigenvalues are equal to $1/\sqrt{c_i}$. This representation will be used to calculate the evolution of the orientation of the lamella system;

(iv) the shape change (and the rotation) of the ellipsoid representing a lamella is obtained from the deformation history by means of the usual formulas of continuum mechanics. The deformation history is described by a prescribed macroscopic velocity gradient **L**, which will in general be time-dependent.

For reasons of convenience, Eq. (21) is re-written in matrix form:

$$[x]^{\mathrm{T}}[C][x] = [1]. \tag{22}$$

Consider a time increment $\Delta t$ (which, during the simulation of a large strain, corresponds to a strain increment). Let $F_{ij}$ be the deformation gradient describing the total change of the ellipsoid during this increment. This means that:

$$[y] = [F][x] \tag{23}$$

in which $x_i$ are co-ordinates of point on the ellipsoid before the time increment, and $y_i$ after. This relation can easily be inverted. This allows

for an expression of Eq. (22) in terms of $y_i$:

$$[y]^{\mathrm{T}}[F^{-1}]^{\mathrm{T}}[C][F^{-1}][y] = [1] \tag{24}$$

or

$$[y]^{\mathrm{T}}[C'][y] = [1] \tag{25}$$

with

$$[C'] = [F^{-1}]^{\mathrm{T}}[C][F^{-1}]. \tag{26}$$

The two latter equations show that $C'_{ij}$ represents the new shape (including orientation) of the ellipsoid after the time step and corresponding strain increment. The orientation of the new axes $x_i^{\ell}$ and the new lengths are obtained by calculating the eigenvectors and eigenvalues of $C'_{ij}$. In practice, $F_{ij}$ must be obtained from $L_{ij}(t)$. This can be done as follows. Textbooks for continuum mechanics give the following classical formula relating them:

$$[L] = [\dot{F}][F^{-1}]. \tag{27}$$

This can be re-written as:

$$[\dot{F}] = [L][F]. \tag{28}$$

Since $L_{ij}$ is known as a function of time, this equation can be integrated to obtain $F_{ij}$ at the end of a time interval $\Delta t$.[7] In the current version of the Lamel software, the integration is done explicitly, which means that $L_{ij}$ is kept constant *during* the time interval $\Delta t$.

### *4.4.3. Organisation of a Simulation*

In the present software, the calculation is organised per time increment (which is equivalent as per strain increment). The calculation of the lattice rotations must be completed for all stacks of two grains before the simulation of the next time increment is initiated. It is possible to vary

[7] Note that in the present context, its initial value at the beginning of the time interval is the unit tensor $\delta_{ij}$.

the prescribed macroscopic velocity gradient tensor **L** for each time increment. The time increments which have been chosen in the present work correspond to an elongation in rolling direction of 2.5%. It is possible to create files with the current texture after each time increment. Such files have been used to generate the ODF of the simulated deformation textures according to the procedure explained in Section 2.

### 4.5. First Results

The cold rolling textures shown by Figs. 3 and 4 have been reproduced using the Lamel model. The procedures described in Section 2, "Validation Strategy", have been used. The hot rolling texture shown by Figs. 1 and 2 has been discretised into 2000 crystallite orientations, of which 1000 stacks of 2 grains have been taken. These were used as "initial stacks" by the Lamel model. Forty-eight deformation steps of a true strain of 2.5% each have been simulated. This corresponds to a thickness reduction of 70%. Figures 13 and 14 show the pole figures ({1 1 0} and {1 0 0}) and the ODF, respectively. Visually, these figures compare well to the experimental results shown by Figs. 3 and 4. However, a quantitative comparison is necessary. It is made by means of the intensity distribution along the fibre (Fig. 15). This figure is similar to Figs. 6 and 9 described in the previous sections. Figure 16 compares

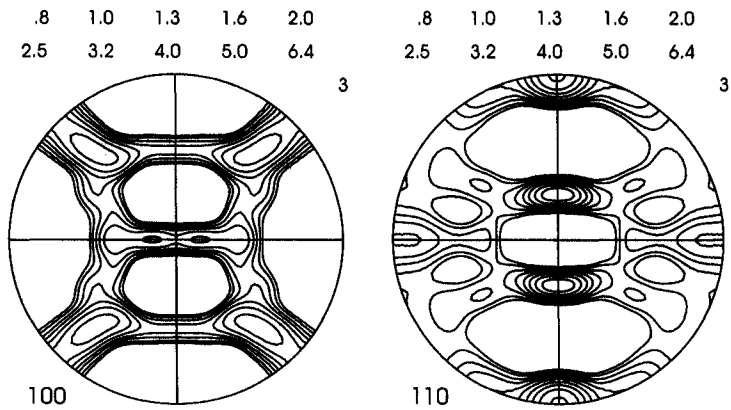


FIGURE 13 {1 1 0} and {1 0 0} pole figures of a cold rolling texture of a b.c.c. material according to the Lamel model. The initial texture is represented by Figs. 1 and 2. A thickness reduction of 70% (true strain: 1.2) has been simulated.

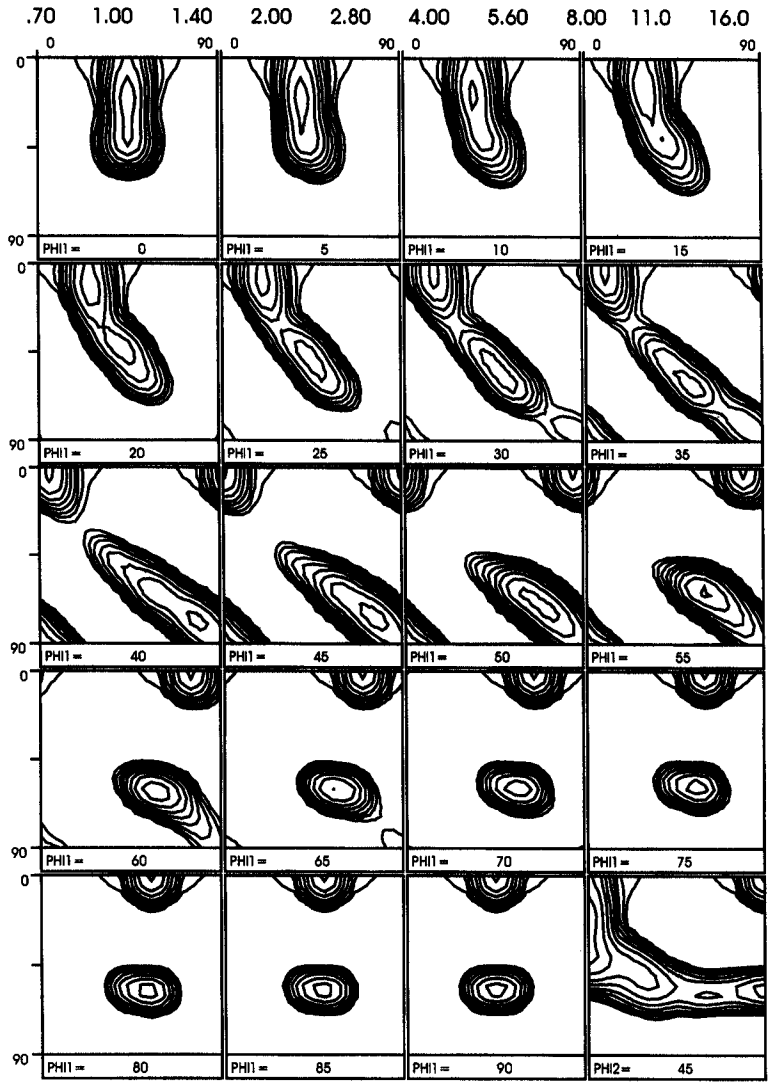


FIGURE 14 ODF of a cold rolling texture of a b.c.c. material according to the Lamel model. The initial texture is represented by Figs. 1 and 2. A thickness reduction of 70% (true strain: 1.2) has been simulated.

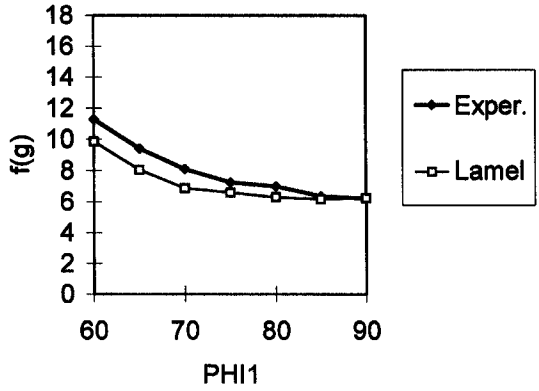


FIGURE 15 Evolution of the maximum intensity along the $\gamma$-fibre for the experimental cold rolling texture and for the results of the Lamel model.

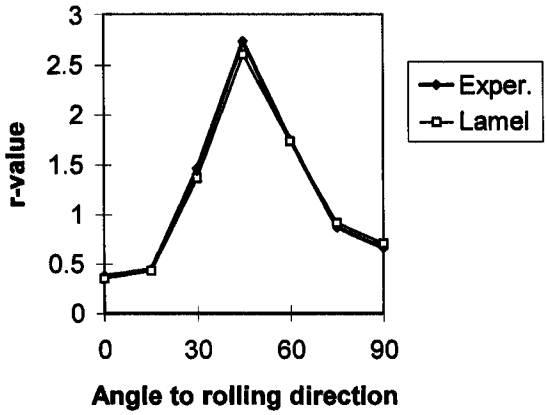


FIGURE 16 $r$-values in function of the angle to the rolling direction, as calculated from the experimental cold rolling steel texture and from the textures simulated by the Lamel model.

the $r$-values as calculated from the texture by means of the FC Taylor theory, and can be compared to Fig. 10, which shows the results of the older models.

Inspection of Fig. 15 reveals a result which is better than expected: not only the *relative evolution* of the values of the ODF along the $\gamma$-fibre is well predicted, but the *level* as well. At one end ($\varphi_2 = 60°$), the Lamel model prediction is 13% lower than the experimental value, and at

$\varphi_2 = 90°$, the two values differ less than 0.5%. This result is much better than any of the results of the older models (Fig. 9).[8] The *r*-values calculated from the texture predicted by the Lamel model are for all practical purposes identical to those obtained from the experimental texture (Fig. 16), which means that they are slightly better as those from

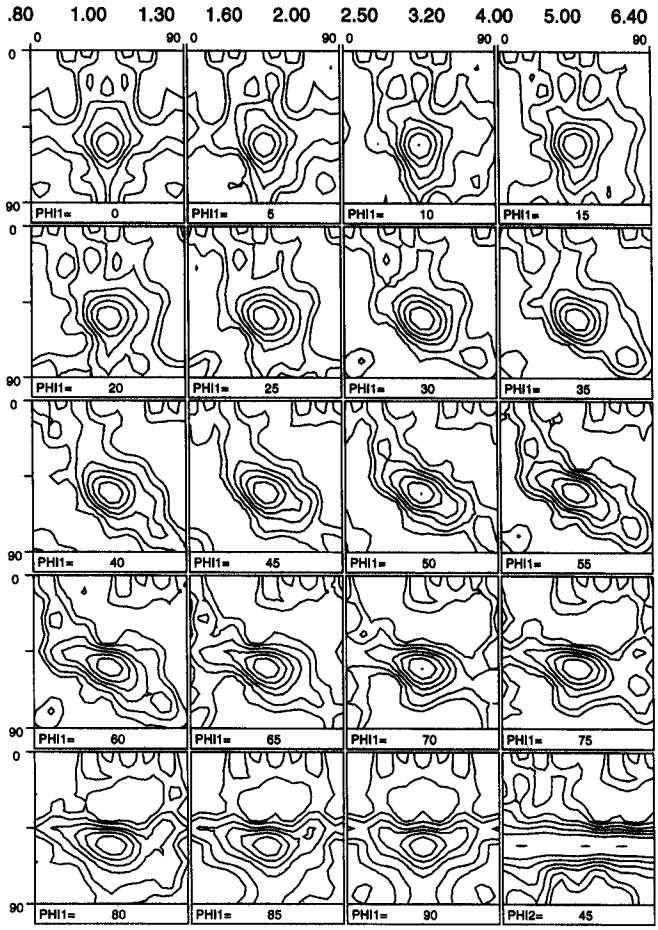


FIGURE 17 ODF of another hot rolled steel, used as initial texture for a second case study.

[8] It is recalled here, that none of the older models referred to in Fig. 9 used adjustable parameters.

the Pancake model, and much better as those from the other older models (Fig. 10).

This first result looked very promising, but it could have been an exceptional case. Therefore it was decided to perform more tests. One of them was already completed at the moment of the preparation of the present paper and will also be reported. It is again a case of cold rolling of steel, but this time starting from a totally different texture (Fig. 17). Compared to the previous initial texture (Fig. 2), this one is much weaker and has a $\gamma$-fibre which is stronger than the $\alpha$-fibre instead of the other way around.

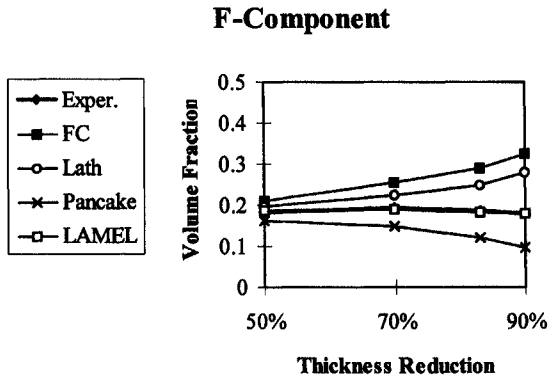


a b

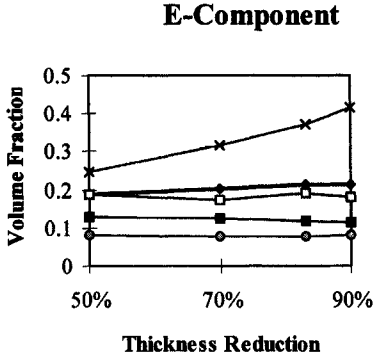


c

FIGURE 18

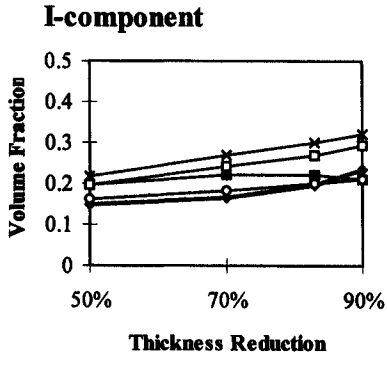


d

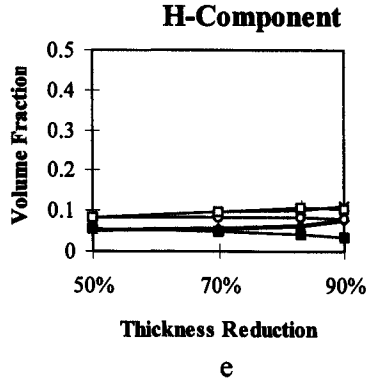


e

FIGURE 18

FIGURE 18 Evolution of volume fractions of rolling texture components as a function of thickness reduction. Initial texture: see Fig. 17. Results of experimental rolling texture and the predictions by the FC, Lath (RC), Pancake (RC) and Lamel model. (a) Legend; (b) (1 1 1)[1 1 $\bar{2}$] (the experimental curve is completely covered by the curve for the Lamel model); (c); (1 1 1)[0 $\bar{1}$ 1]; (d); (2 1 1)[0 $\bar{1}$ 1] (e); (1 0 0)[0 $\bar{1}$ 1] (the curve for the Pancake model is completely covered by the curve for the Lamel model). Note that the first two components belong to the $\gamma$-fibre, and the two last to the $\alpha$-fibre.

Figure 18 shows the results in terms of volume fractions, calculated by convoluting the ODF with appropriate Gauss distributions (Van Houtte, 1992). Results are given for 50%, 70%, 83% and 90% thickness reduction. Again, the Lamel model clearly outperforms the other models for volume fractions of texture components belonging to the $\gamma$-fibre.

The results are less convincing for texture components belonging to the $\alpha$-fibre. The Lamel model tends to overestimate the volume fraction, whereas the FC and Lath model perform better.

## 5. DISCUSSION

The Lamel models has some similarities with the "Deformation Banding" model published by Lee *et al.* (1993; 1995) and the "Grain Subdivision" model proposed by Leffers (1994). In these models, which were intended to model the plastic deformation and the deformation texture development of f.c.c. metals, each grain is subdivided in two families of lamellar bands (deformation bands). There are $2n$ bands in each grain, $n$ being a number equal to or larger than 1. Bands of the two families are alternating. In a geometrical way, a pair of such bands (one of each family) is identical to a stack of two grains as shown in Fig. 12, and also has free shears of equal amplitude but opposite signs in the two bands. The differences with the Lamel model are that grain 1 and grain 2 of the latter do not necessarily represent bands inside a grain (although the model could be used in such way, see below), and that a different choice is made for the orientation of the boundary plane between the lamellae (lamella reference system). In the "Grain Subdivision model" (Leffers, 1995), the lamellae are parallel (or nearly parallel) to the transverse direction as is the case for the Lamel model as applied in the present paper, but the angle between the lamellae and the rolling direction is not zero. As far as the present authors can judge, the kinematic equations of the "Grain Subdivision model" (Leffers, 1995) are essentially equivalent to those of the Lamel model. According to the "Deformation Banding" model (Lee *et al.*, 1993; 1995), the lamella planes are normal to the transverse direction, so their orientation is totally different than in the "Grain subdivision model" or in the Lamel model. Moreover, the "Deformation Banding" model uses the classical Pancake model as a starting basis. So $l_{13}$ and $l_{23}$ (using the axis conventions of the present paper) are relaxed first. Next, alternating free shears of the type $l_{12}$ are allowed in the bands. In their mathematical treatment, the authors try to take energetic effects due to latent hardening, misorientation between deformation bands and the accommodation of the misfits into account. Only misfits which are expected at the end of their deformation bands are

considered. Their accommodation is treated as an elastic problem. However, they do not bother about the strain misfits inherent to the pancake model. A problem with the two "banding" models (Lee *et al.*, 1993; 1995; Leffers, 1994) seems to be, that when the two bands have exactly the same crystallite orientation, the energetic advantage that a relaxation shear may have in the bands of family 1 is exactly compensated by an energetic disadvantage in family 2, at least when using a first-order analysis. The problem could be resolved by considering a slight misorientation between the two families. An additional model which could explain/predict such misorientations would be helpful. However, a complete discussion of this aspect would be beyond the scope of the present paper. To the best knowledge of the present authors, neither the "Grain Subdivision model" (Leffers, 1994) nor the "Deformation Banding" model (Lee *et al.*, 1993; 1995) has been used for quantitative texture predictions of the rolling texture of b.c.c. metals.

The success of the Lamel model as depicted above should be put into perspective. First note that so far, the validation has only been done for the case of cold rolling of low-carbon steel (as a representative of b.c.c. metals). It cannot be taken for granted that a similar success would be achieved for other cases, such as other deformation modes applied to steel, or any deformation mode applied to f.c.c. or h.c.p. metals. It is planned to test these cases too, using validation procedures as described in Section 2, but this will take some time.

Secondly, it should be noted that although excellent results have been obtained for the components of the $\gamma$-fibre, the same cannot be said for those belonging of the $\alpha$-fibre. The success for the $\gamma$-fibre is amazing: not only the relative intensities and volume fraction have been well predicted quantitatively, but also the absolute level of the volume fraction. The first aspect could be achieved if the model merely gives a good prediction of the rotations of grains belonging to the $\gamma$-fibre. The second aspect really means that the evolution of relative weight of the $\gamma$-fibre with respect to all other texture components is also well predicted; this involves a good simulation of rotation rates of grains flowing in or out of the $\gamma$-fibre. In view of this latter aspect, it is surprising that the model clearly overestimates the volume fractions of the $\alpha$-fibre (Fig. 18(d) and (e)). Perhaps it is the *spread around the ideal fibre* axis which is larger in the real material than in the simulated results. This could be explained if the grain orientations of the $\alpha$-fibre would be subject to a larger

randomisation effect due to local strain heterogeneities as compared to the grains of the $\gamma$-fibre. It is true that the latter are the "hard" orientations, whereas some of the $\alpha$-orientations are rather soft, and can therefore be expected to be forced to accommodate strain misfits caused by strain relaxations of the hard grains. This aspect might be studied experimentally by means of a scanning electron microscope equipped with an EBSD-attachment.

The surprising quality of the $r$-value predictions (Fig. 16) seems to indicate that as regard to mechanical properties, the influence of the $\gamma$-fibre is dominating, so that errors on the volume fractions of the $\alpha$-fibre do not matter much.

On the whole, one may wonder which aspect of the local stress and strain distributions it is, which is so well captured by the Lamel model that it leads to deformation texture predictions which even have a good quantitative agreement. In Section 4.2, it was argued that the accommodation of the misfit strains between neighbouring grains caused by the Lamel model would be easier than would be the case for the Pancake model or even the Generalised Relaxed Constraints model. This argument does not really convincingly explain the success of the model. Maybe the real reason is that the model satisfies stress equilibrium (as regard to the shear stress components $\sigma'_{13}$ and $\sigma'_{23}$) at the boundaries between grain 1 and grain 2, i.e. the grain boundary with the largest surface of pancake-shaped grains. Indeed, this result was found during the mathematical analysis of the Lamel model, see Eq. (20) and the comments in Section 4.3. Note that the Pancake model also achieves this kind of stress equilibrium by requiring that $\sigma'_{13}$ and $\sigma'_{23}$ are zero in all grains. This is probably a too strong condition; the Lamel model only requires that these shear stress components must be equal at both sides of the grain boundary.

The problem of the accommodation of the strain misfit remains. Figure 12 shows a stack of two grains in which some relaxation took place as assumed by the Lamel model. Assume that this stack as a whole would be an inclusion in a homogeneous matrix. Then the accommodation of the misfit strain would require a heterogeneous deformation pattern in the matrix around the stack which has as net result that some material is transferred from the region around D′ to the region around C′ (Fig. 12). This would still require an important additional plastic work, although (for the same relaxation shear) less than for other

models such as Pancake or Generalised RC. It is more likely that in the microstructure, some patterns of heterogeneous deformation exist which link up sites such as C′ and D′ in different stacks of two grains in different planes which are in each other's vicinity, and might allow for misfit accommodation at rather short range. Such patterns may have a wavy aspect, or might look like short, diffuse shear bands.

A further problem of interpretation is the identification of the "stacks of two grains" as depicted in Fig. 11 with some features of the microstructure. It was taken for granted in this paper that "grain 1" and "grain 2" are flat, elongated grains; but perhaps it would be better to identify them with microbands, deformation bands or even slip bands with in a grain. Clarification of this point will also require experimental investigations of deformed microstructures. If it turns out to be true that one must identify grain 1 and grain 2 with deformation bands within the same grain, then the texture predictions for the $\alpha$-fibre would be different. Indeed, as the $\alpha$-fibre forms a minority, it is very unlikely that in the present simulation scheme, for both grain 1 and grain 2 an orientation of the $\alpha$-fibre would be taken. In the simulation scheme, a grain of the $\alpha$-fibre will most of the time find itself in presence with one of the $\gamma$-fibre, which will probably enforce its relaxation since it has the "harder" orientation. On the other hand, in a "deformation banding" model, an $\alpha$-orientation would be coupled with another one,[9] which would almost certainly would lead to a different simulation result.

A last comment is devoted to the model itself. The present Lamel model works with stacks of two grains which have two degrees of freedom, i.e. 1 degree of freedom per grain on average (instead of 2 in the Pancake model). Of course one could imagine a model which would work with stacks of three or more grains. It can easily be seen, that the more grains one takes, the higher the ratio between the number of degrees of freedom to the number of grains becomes; this ratio will tend to 2 (as in the Pancake model) if the number of grains tends to infinity. Predictions of such models will hence be intermediary between those of the Pancake model and those of the Lamel model.

[9] Initially, they would almost have the same orientation, since separated by a low-angle boundary.

Other models have been proposed in which the orientation of the boundary between grain 1 and grain 2 is left free (whereas in the Lamel model, it is prescribed by the user). It would be interesting to compare the results of the two types of models.

## 6. CONCLUSIONS

It was found, that reliable quantitative predictions of the intensity and volume fraction of the $\gamma$-fibre texture components of the rolling textures of low-carbon steel are possible by means of the Lamel model. $r$-Values derived from the predicted textures are almost identical to those derived from the experimental textures, in spite of the fact that $\alpha$-fibre texture components are overestimated by the new model.

At present, there is no proof that the same quality of prediction will be achieved in other cases, such as the rolling textures of f.c.c. metals. Such tests need to be done in future work. It will also be attempted to assess the physical assumptions made by the Lamel model as regard to microscopic strain heterogeneity. This work will be done by investigating rolled samples by means of scanning electron microscope equipped with an EBSD attachment. The interpretation of the results in terms of the Lamel model will be greatly facilitated by the fact that the latter model is based on simple physical assumptions which do not involve the fine tuning of adjustable parameters.

### *Acknowledgements*

Financial support for this work has been obtained from the Federal government of Belgium (DWTC) through the contract IUAP P4/33, and from the 'Fonds voor Wetenschappelijk Onderzoek – Vlaanderen' (FWO) through the research contract G.0252.96. One of the authors (L.D.) acknowledges his grant as 'aspirant' of the FWO.

The company Sidmar-OCAS has supplied test material and has carried out rolling operations, which is gratefully acknowledged.

### *References*

Aernoudt, E., Van Houtte, P. and Leffers, T. (1993). Deformation and textures of metals at large strains. In *Plastic Deformation and Fracture of Materials* (Vol. 6 of *Materials*

*Science and Technology: A Comprehensive Treatment*, edited by R.W. Cahn, P. Haasen and E.J. Kramer), edited by H. Mughrabi, pp. 89–136. Weinheim, Federal Republic of Germany: VCH.

Bunge, H.J. (1982). *Texture Analysis in Materials Science*, London: Butterworth.

Gil Sevillano, J., Van Houtte, P. and Aernoudt, E. (1980). Large strain work hardening and textures, *Progr. Mat. Sci.*, **25**, 69–412.

Honeff, H. and Mecking, H. (1981). Analysis of the deformation texture at different rolling conditions. In *Proc. ICOTOM 6*, Vol. 1, edited by S. Nagashima, pp. 347–355. Tokyo: The Iron and Steel Institute of Japan.

Kocks, U.F. and Chandra, H. (1982). Slip geometry in partially constrained deformation. *Acta Metall.*, **30**, 695–709.

Lee, C.S., Duggan, B.J. and Smallman, R.E. (1993). A theory of deformation banding in cold rolling. *Acta Metall. Mater.*, **41**, 2265–2270.

Lee, C.S., Smallman, R.E. and Duggan, B.J. (1995). A simplified criterion for deformation banding applied to deformation texture simulation. *Scripta Metall. Mater.*, **33**, 727–733.

Leffers, T. (1994). Lattice rotations during plastic deformation with grain subdivision. In *Proc. 10th Intntl. Conf. on Textures of Materials (ICOTOM 10)*, Clausthal, Germany (20–24 September 1993), edited by H.J. Bunge, *Materials Science Forum* **157–162**, 1815–1820.

Leffers, T., Asaro, R.J., Driver, J.H., Kocks, U.F., Mecking, H., Tomé, C. and Van Houtte, P. (1988). Deformation textures: simulation principles. In *Proc. of the Eighth Int. Conf. on Textures of Materials*, edited by J.S. Kallend and G. Gottstein, pp. 265–272. Warrendale, Pennsylvania: The Metallurgical Society.

Molinari, A., Canova, G.R. and Ahzi, S. (1987). A self-consistent approach of the large deformation polycrystal viscoplasticity. *Acta Metall.*, **35**, 2983–2994.

Schouwenaers, R., Van Houtte, P., Aernoudt, E., Standaert, C. and Dilewijns, J. (1994). Prediction of the plastic anisotropy of low carbon steel sheet by means of Taylor-modelling. *ISIJ International*, **34**, 366–372.

Taylor, G.I. (1938). Plastic strain in metals. *J. Inst. Metals*, **62**, 307–324.

Toth, L.S. and Van Houtte, P. (1992) Discretization techniques for orientation distribution functions. *Textures and Microstructures*, **19**, 229–244.

Toth, L.S., Van Houtte, P. and Van Bael, A., (1991). Analytical representation of polycrystal yield surfaces. In *Anisotropy and Localization of Plastic Deformation (Proc. Plasticity '91: 3rd Int. Symp. on Plasticity and its Current Applications)*, edited by J.P. Boehler and A.S. Khan, pp. 183–186. London: Elsevier Applied Science.

Van Houtte, P. (1982). On the equivalence of the relaxed Taylor theory and the Bishop–Hill theory for partially constrained plastic deformation of crystals. *Mater. Sci. Eng.*, **55**, 69–77.

Van Houtte, P. (1988). A comprehensive mathematical formulation of an extended Taylor–Bishop–Hill model featuring relaxed constraints, the Renouard–Wintenberger theory and a strain rate sensitivity model. *Textures and Microstructures*, **8–9**, 313–350.

Van Houtte, P. (1991). A method for the generation of various ghost correction algorithms – the example of the positivity method and the exponential method. *Textures and Microstructures*, **13**, 199–212.

Van Houtte, P. (1992). *Manual of the MTM-FHM software*. K.U. Leuven: Department MTM.

Van Houtte, P. (1995). Heterogeneity of plastic strain around an ellipsoidal inclusion in an ideal plastic matrix, *Acta Metall. Mater.*, **43**, 2859–2879.

Van Houtte, P. (1997). Micromechanical models for the prediction of deformation textures. In *Proc. NASAT-97*, edited by A.K. Singh. Kanchanbach, Hyderabad, India: Defence Metallurgical Laboratory.

Van Houtte, P. and Rabet, L. (1997). Generalisation of the relaxed constraints models for the prediction of deformation textures. *Revue de Métallurgie -CIT/Science et Génie des Matériaux*, **94**, 1483–1494.

Vanderschueren, D., Van Houtte, P., Aernoudt, E., Dilewijns, J. and Standaert, C. (1994). Hot rolling textures of low carbon steel sheets and their influence on the texture after continuous annealing. In *Advances in Hot Deformation Textures and Microstructures*, edited by J.J. Jonas, T.R. Bieler and K.J. Bowman, pp. 95–106. Warrendale, Pennsylvania, USA: TMS.